Article

Twisted Silica Few-Mode Hollow GeO_2-Doped Ring Core Microstructured Optical Fiber

Anton V. Bourdine[1,2,3,4]*, Vladimir V. Demidov[2], Egishe V. Ter-Nersesyants[2], Grigori A. Pchelkin[2,4], Dmitriy N. Shurupov[2,5], Alexander V. Khokhlov[2], Alexandra S. Matrosova[2], Andrey I. Kashin[2], Sergei V. Bureev[2], Michael V. Dashkov[1], Alexander S. Evtushenko[1], Elena S. Zaitseva[1], Azat R. Gizatulin[7], Ivan K. Meshkov[7], Amogh A. Dyavangoudar[8], Ankur Saharia[8], Manish Tiwari[8], Alexander A. Vasilets[9], Vasiliy S. Elagin[4], Ghanshyam Singh[10], Konstantin V. Dukelskii[2,4,10]

1 Department of Communication Lines, Povolzhskiy State University of Telecommunications and Informatics, 23, Lev Tolstoy street, Samara 443010, Russia; bourdine@yandex.ru (A.V.B.), mvd.srttc@gmail.com (M.V.D.), alex2194ru@yandex.com (A.S.E.), zaytzewa@inbox.ru (E.S.Z.)
2 JSC "Scientific Production Association State Optical Institute Named after Vavilov S.I.", 36/1, Babushkin street, St. Petersburg 192171, Russia; demidov@goi.ru (V.V.D.), ter@goi.ru (E.V.T-N.), beegrig@mail.ru (G.A.P.), shurupoff.dm@yandex.ru (D.N.S.), khokhlov@goi.ru (A.V.Kh.), a.pasishnik@gmail.com (A.S.M), kashin_andrey@mail.ru (A.I.K.), bureev@goi.ru (S.V.B.), kdukel@mail.ru (K.V.D.)
3 "OptoFiber Lab" LLC, Skolkovo Innovation Center, 7, Nobel street, Skolkovo Innovation Center, Moscow 143026, Russia;
4 Department of Photonics and Communication Links, Saint Petersburg State University of Telecommunications named after M.A. Bonch-Bruevich, 22, Bolshevikov avenue, St. Petersburg 193232, Russia; elagin.vas@gmail.com (V.S.E.)
5 Institute of Physics, Nanotechnology and Telecommunications, Peter the Great St. Petersburg Polytechnic University, bldg. II, 29, Politekhnicheskaya str., St. Petersburg 194064, Russia
6 Department of Telecommunication Systems, Ufa State Aviation Technical University, 12, Karl Marx Street, Ufa 450000, Russia; azat_poincare@mail.ru (A.R.G.); mik.ivan@bk.ru (I.K.M.)
7 Optoelectronics and Photonics Research Lab, Department of Electronics and Communication Engineering, Manipal University Jaipur, 303007, India; amogh.199202014@muj.manipal.edu (A.A.D.); ankur.saharia@jaipur.manipal.edu (A.S.); manish.tiwari@jaipur.manipal.edu (M.T.)
8 Dept. of Electronics and Communication Engineering, School of Electrical and Electronics & Communication Engineering, Malaviya National Institute of Technology, J.L.N Road, Jaipur 302017, Rajasthan, India; gsingh.ece@mnit.ac.in (G.S.)
9 Dept. of Physics and Mathematics Branches of Science and Information Technologies, Volga Region State University of Physical Culture, Sport and Tourism, 35, Universiade Village, Kazan 420010, Rep. Tatarstan , Russia; a.vasilets@mail.ru (A.A.V.)
10 Faculty of Photonics and Optical Information, School of Photonics, ITMO University, bldg. A, 49, Kronverksky alley, St. Petersburg 197101, Russia
* Correspondence: bourdine@yandex.ru

Abstract: This work presents first time successfully fabricated silica few-mode microstructured optical fiber (MOF) with hollow GeO_2-doped ring core and strongly induced twisting up to 790 revolutions per meter. Some technological issues for manufacturing of GeO_2-doped supporting elements for large hollow cores as well as described above complicated spun MOFs are discussed. We introduce some results of tests, performed for pilot samples of designed and manufactured described above untwisted and twisted MOFs with outer diameter 65 μm and hollow ring core inner diameter 30.5 μm under wall thickness 1.7 μm and refractive index difference Δn=0.030, including their geometrical parameters, basic transmission characteristics and measurements of far-field laser beam profile patterns.

Keywords: hollow ring core fiber; twisted microstructured optical fiber; chirality; silica GeO_2-doped supporting elements; laser beam profile; laser-based few-mode optical signal transmission

1. Introduction

Preprints (www.preprints.org) | NOT PEER-REVIEWED | Posted: 25 May 2023 doi:10.20944/preprints202305.1814.v1

Typical hollow (or air) ring core (HRC) optical fibers differ by large single silica hollow core with doped walls (or drawn from supporting capillary, fabricated from special optical glass / material with refractive index material higher, than pure silica) to provide great refractive index difference between air in hollow core, core walls and outside silica cladding, that affords unique optical waveguide properties. Nowadays, HRC microstructured optical fibers (MOFs) / photonic crystal fibers (PCFs) as well as pure HRC optical fibers are primely targeted for generation, maintenance and transmission of orbital angular momentum (OAM) modes in optical telecommunication systems, based on spatial (e.g. mode) division multiplexing (SDM / MDM) technique [1-3]. Also, this type of optical fibers is declared as mode converters for differential mode delay reduction in laser-based multi-Gigabit data transmission short range optical networks with multimode optical fibers [4, 5], higher-order mode dispersion compensation [5, 6] and acousto-optic control of polarization [5].

Presented work is exactly focused on described above HRC optical fiber geometry, while there are other groups of other well-known both "initial" ("basic") and "spin-off" following similar fiber optic structures, containing:

– ring (or annular) core optical fibers (pure silica core and cladding with inclusion of high refractive index material layer on core / cladding boundary) [1-3, 7-13 et al.];

– ring core MOFs and PCFs (silica center, bounded by ring from higher refractive index material / glass (doped silica), and air holes in periphery) [14, 15];

– hollow core MOFs and PCFs, also known as hollow core photonic bandgap fibers (pure silica circular fiber with large air central hole (e.g. "core") and small air holes in periphery part, placed according to desired designed geometry) [1, 2, 16-31 et. al.];

– anti-resonant hollow core fiber (AR-HCF) with complicated geometry: so-called "revolver" fibers – single / double / triple ring AR-HCF and single / double noodles nested AR-HCF [3, 29, 32-34 et al.] and nodeless nested AR-HCF [3, 29, 32, 33, 35, 36 et al.], "grapefruit" [37, 38 et al.], "ice-cream" [29, 39 et al.].

There is a set of known published works, focused on design and simulation of HRC MOFs, that guide and support propagation of various number of OAM modes: 146 and 70 modes at λ=1100 nm and 2000 nm, respectively (HRC MOF with total outer diameter 116 μm, 4 μm air core, bounded by phosphate optical glass ring with wall thickness 2 μm and difference between doped ring and pure silica refractive indexes Δn=0.11) [40], 180 OAM modes over λ=1500…1700 nm wavelength band (HRC MOF with total outer diameter 116 μm, air core diameter 51 μm, ring wall thickness 1.5 μm with Δn=0.12 (analogue to FBG1 glass – 56.7% SiO_2, 0.35% Al_2O_3, 30% PbO, 4.15% Na_2O, and 8.65% K_2O)) [41], 22 OAM modes at λ=1550 nm (HRC PCF with total outer diameter 28 μm, 11 μm air core, bounded by lanthanide (LaSF09) optical glass ring with wall thickness 0.1 μm and Δn=0.37) [42], 436 at λ=1550 nm with 400 modes over S+C+L bands (203 μm HRC optical fiber with 100 μm hollow ighly-GeO_2-doped-ring-core under ring wall thickness 1.5 μm and Δn=0.15) [43], 874 OAM modes at λ=1550 nm with 514 modes over almost all telecommunication band (62.5 μm HRC PCF with 20 μm air core, bounded by As_2S_3-ring with wall thickness 0.5 μm and extremely high Δn=1.00) [44] and up to 1004 OAM modes over extended wavelength range, covering almost all ratified telecommunication bands (O, E, S, C, L), under record high number of 1346 OAM modes at λ=1550 nm (62.5 μm HRC optical fiber with 20 μm air core, bounded by As_2S_3-ring with wall thickness 0.9 μm and extremely high Δn=1.00) [45].

It is obviously, earlier on published papers, containing not only simulation, but primarily results of tests, performed for successfully fabricated designed optical fibers, are of special interest. However, in spite of declared HRC MOF great potentiality for guiding and transmission of OAM modes [1 – 3, 40 – 45], there are not so much reports, presenting properties, results of tests and measured data of manufactured HRC fibers. Finally, there is just a set of works, prepared by group of the same authors, that shew experimentally verified ability of stable transmission for 12 OAM modes over C-band along designed and fabricated HRC optical fiber with air core diameter 6 μm, bounded by ring with wall thickness 5.25 μm and Δn=0.03 [3, 46 – 49] with following enhancing supporting AOM mode

Preprints (www.preprints.org) | NOT PEER-REVIEWED | Posted: 25 May 2023 doi:10.20944/preprints202305.1814.v1

quantity up to 28 by enlarging air core diameter up to 19 μm under the same ring parameters [50]. While other "experimental" papers present propagation of OAM modes over ring core optical fibers [1 – 3, 9, 10, 51 – 53] and hollow core "grapefruit" MOF [3, 54, 55]. In addition, twisted or spun MOFs and PCFs are not only declared as new (alternative to primarily fiber Bragg gratings) type of fiber optic probes for sensors of strain / twisting [56 – 58] and magnetic field / electric current [59] or special optical fibers for polarization maintenance, generation of optical activity [60 – 65] or mode filtration [66], but also, they are positioned as new optical fibers with great potentiality for guiding and transmission of OAM modes, which was confirmed by not only theoretical simulations [3, 67 – 71], but also by experimental researches [72 – 77]. This work presents results of attempt to combine all described above fiber optic structures: hollow core MOF, ring hollow core optical fiber and twisted MOF. First time, we successfully fabricated silica few-mode MOF with hollow GeO_2-doped ring core and strongly induced twisting up to 790 revolutions per meter. Some technological issues for manufacturing of GeO_2-doped supporting elements for large hollow cores as well as described above strongly twisted MOFs are discussed. We introduce some results of tests, performed for pilot samples of designed and manufactured described above untwisted and twisted MOFs with outer diameter 67 μm and hollow ring core inner diameter 25 μm under wall thickness 0.85 μm, including their geometrical parameters, basic transmission characteristics and measurements of far-field laser beam profile patterns.

2. Fiber Design

Proposed HRC MOF pilot design is represented on Figure 1. It is composed of central hollow air core with radius r_1, bounded by GeO_2-doped silica ring with outer radius r_2 and wall thickness $\Delta r = (r_2 - r_1)$. There are 108 air holes with inner radius r_3 and pith Λ, placed over hexagonal geometry in the periphery part of fiber, which forms total proposed HRC MOF structure with outer radius r_4.

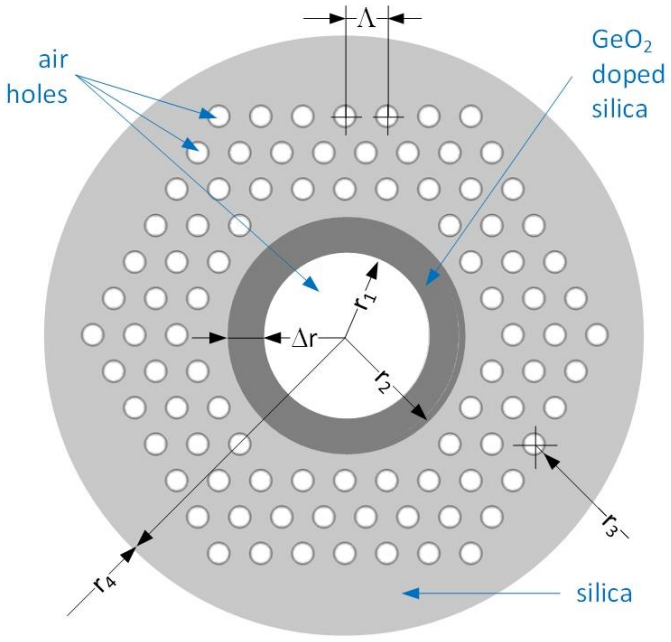

Figure 1. Proposed hollow GeO_2-doped ring core MOF design.

We utilized rigorous numerical full-vectorial Finite-Element-Method by using commercially available COMSOL Multiphysics® software for preliminary modal analysis of designed GeO_2-doped HRC MOF under following preliminarily chosen parameters: hollow core inner radius r_1=5 μm; GeO_2-doped ring wall thickness Δr=4 μm (HRC outer radius is r_2=9 μm); GeO_2-doped ring and pure silica difference of refractive indexes Δn=0.03;

Preprints (www.preprints.org) | NOT PEER-REVIEWED | Posted: 25 May 2023 doi:10.20944/preprints202305.1814.v1

air hole radius r_3=1.7 μm; pitch Λ=3.25 μm. Modal analysis was performed at the wavelength λ=1550 nm. Here GeO_2-doped ring refractive index value was estimated by well-known Sellmeier equation [78 et al.] with substituted coefficients, experimentally measured for GeO_2-SiO_2 glasses [79, 80] under particular dopant concentrations, while unknown can be evaluated by earlier on developed method [81].

OAM modes can be obtained by combination of eigenmodes ("even" and "odd" modes) with a π/2 phase shift, that is described by well-known summarized expressions [1 – 3, 7 – 45 et al.]. Therefore, two OAM modes are localized and supported by proposed designed and simulated HRC MOF (Figure 2).

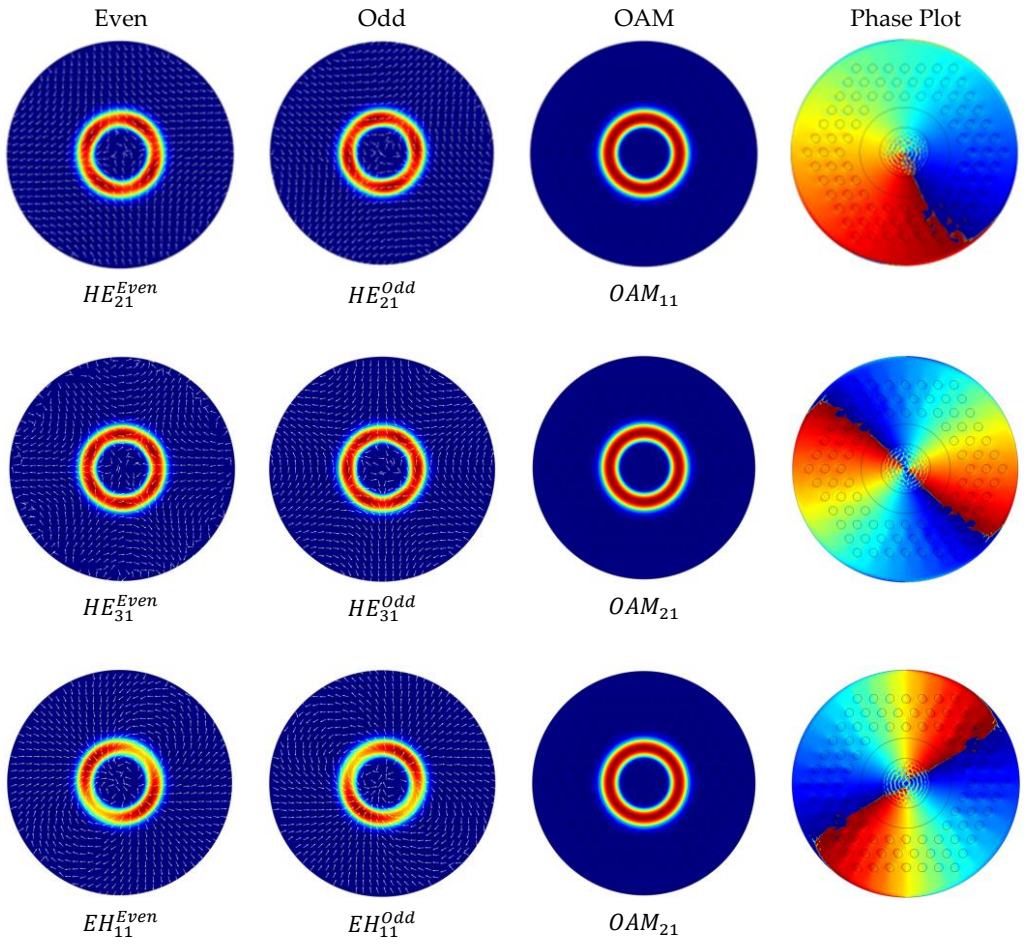

Figure 2. OAM mode formation by combined even and odd eigenmodes of designed HRC MOF.

3. Fabrication of GeO_2-Doped Supporting Tubes – Preforms of Hollow Ring Core

We applied conventional modified chemical vapor deposition (MCVD) method for fabrication of silica supporting tubes with GeO_2-doped walls, which are preforms of hollow ring cores. Here commercially available basic silica supporting tubes with outer diameter 22 mm, wall thickness 2 mm, length 650 mm were used as basic element for HRC preforms. These cheap supporting tubes have high OH^--group concentration (it is more than 1000 ppm—analog to the brands Heraeus Suprasil Standard, Saint-Gobain Spectrosil A and B, Corning HPFS 7980, JGS1, Dynasil 1100/Dynasil 4100, Russian GOST 15130-86 "Optical quartz glass" KU-01, etc.), while it provides ability for low temperature MCVD-process operation to avoid tube deformation and redundant evaporation of highly GeO_2-doped quartz near-surface layers.

Developed and verified technological process for fabrication of GeO_2-doped silica tubes contains the following sequential steps:

Preprints (www.preprints.org) | NOT PEER-REVIEWED | Posted: 25 May 2023 doi:10.20944/preprints202305.1814.v1

1. Flushing of supporting tube in distilled water with further drying under normal conditions.
2. Installation of supporting tube in the chucks of MCVD station.
3. Supplying SF6 gas to the inside of the tube for chemical etching of distorted near-surface quartz layers.
4. Deposition of phosphor-silicate quartz layers to prevent the diffusion of OH-groups from the supporting tube to the germane-silicate quartz layers.
5. Deposition of germane-silicate quartz layers for an improvement in refractive index and material photosensitivity by the formation of germanium oxygen-deficient centers.

According to mentioned above technological process description, we performed series of several GeO_2-doped supporting tubes experimental fabrication with further redrawing them to capillaries / HRC preforms. As a result, optimal parameters and regimes of technological process were successfully empirically selected:

- Delivering rate and concentration of gas mixture / reagents (in particular, $GeCl_4$ in vapor-gas mixture to prevent bubbles, that lead to further cracking of fabricating supporting element).
- Oxygen torch movement speed and its flame temperature.
- Numbers of torch passes.
- Dried oxygen flow rate (in mm^3 per minute (mm^3/min)), going through the bubbler systems with $GeCl_4$ and $SiCl_4$, during torch passes.
- Ratio between numbers of phosphor-silicate quartz layers (4…9) and germane-silicate quartz layers (20…55).

During the first series of experimental fabrications, 50 numbers of torch passes were selected. However, here we have got supporting tube cracking as yet it was placed in MCVD station chucks, or increased fragility of fabricated capillaries, redrawn from successfully deposited undestroyed tube, that lead to their collapsing under further MOF drawing. After second series of experiments, we detected, that typical dried oxygen flow rate over 400 mm^3/min during its passing through the bubbler system with $GeCl_4$ and 40…50 mm^3/min for $SiCl_4$ bubbler system lead to "boiling" of germane-silicate quartz layers, deposited over insight surface of the tube, or, e.g., occurring of bubbles in GeO_2-doped layer. Therefore, during the third series of experiments, optimal regimes were empirically detected: 50 torch passes, 400 mm^3/min dried oxygen flow rate under going through $GeCl_4$ bubbler system and 105 mm^3/min dried oxygen flow rate under going through $SiCl_4$ bubbler system. Also, we add final deposition of 5 pure quartz layers to prevent the cracking of previously deposited thick germane-silicate quartz layers during preform cooling due to great difference between linear expansion thermal coefficients of pure silica and highly doped germane-silicate quartz.

Therefore, we successfully fabricated preforms for GeO_2-doped HRCs by proposed technique: from supporting tube with deposited germane-silicate quartz layers (Figure 3a,b) under GeO_2-dopant concentration 20.5 mol%, providing desired core-cladding refractive index difference Δn=0.030, and further their redrawing to capillaries.

However, during MOF stack formation another same problem occurred, concerned with cracking of capillary, already placed into the stack. After new series of experiments, we detected, that possible cause of capillary destruction may be explained by fact, that closed (fused) end of capillary extends beyond the outer diameter of supporting element (Figure 3d). During MOF stack formation, supporting elements are densely pack in the outer main supporting tube, so compression between them occurs, that leads to cracking and destruction of GeO_2-doped capillaries due to their increased fragility, explained by also mentioned above difference between linear expansion thermal coefficients of pure silica and highly doped germane-silicate quartz.

We developed and verified an alternative method for fusing (ending) of GeO_2-doped capillary, that provides successful solution of described above problem. Instead of conventional positioning of capillary end face to the side of the oxygen torch flame, we place capillary itself with desired length to the flame, after heating its ends are pull out up to

Preprints (www.preprints.org) | NOT PEER-REVIEWED | Posted: 25 May 2023 doi:10.20944/preprints202305.1814.v1

splitting in the heated place, and formed conical ends are fused (closed) (Figure 3c). As a result, fused ends do not extend beyond outer size of capillary, that eliminates the problem of cracking and destruction of GeO_2-doped capillaries due to compression in dense pack during MOF stack formation.

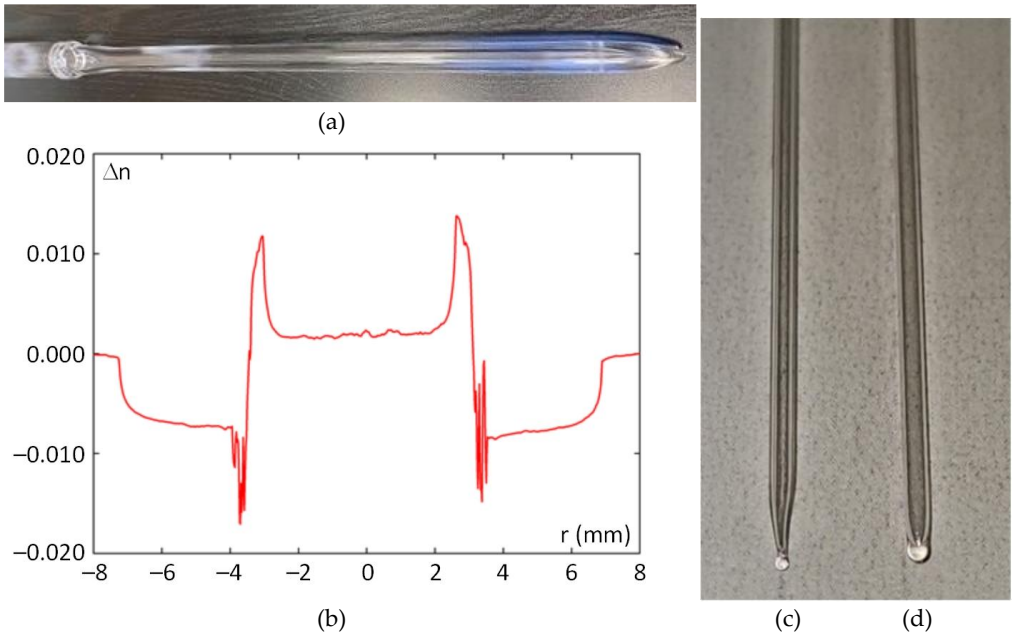

Figure 3. GeO_2-doped silica supporting tube: (a) tube; (b) supporting tube refractive index profile; (c) and (d) fused (closed) ends of GeO_2-doped capillary: (c) by proposed method with splitting; (d) by conventional method.

4. Fabrication of Silica Microstructured Optical Fibers with Improved Induced Twisting

In the earlier on published papers [82 – 88], we described in details all previously successfully performed stages of drawing tower modifications, that provide to improve twisting of fabricated MOF from initial weak 10 revolutions per meter (rpm) up to 66 rpm [82, 83] and further 100, 400 and 500 rpm [87, 88]. We have chosen to develop the method, proposed in [1]: rotation of optical fiber preform during the drawing process.

During the first stage, we installed a stepper motor with rotation speed 200 revolutions per minute to the feed unit of tower to add the rotation option to the drawing system, which provided maximal induced chirality over optical fiber only of 100 rpm under the drawing speed of 2 m per minute. We have designed and fabricated a special fluoroplastic rotational adapter (Figure 4a), that directly connects an excess pressure hose to the top end of the cane and fixes it without twisting, to prevent drops in pressure between the hose and the top end of the cane due to the sealed internal space of the rotational adapter under ability of cane rotation during the MOF drawing with the desired speed. At the same time, we tested, verified and work out the full-cycle technique of twisted MOF fabrication: from MOF stack formation, redrawing it to MOF cane and following MOF drawing from the cane with twisting under specified excess pressure and drawing temperature [82, 83]. During this stage, we successfully fabricated following MOFs with twisting from 10 rpm (rotation speed is 20 revolutions per minute with MOF drawing speed 2 meters per minute) up to 66 rpm (rotation speed is 200 rpm with MOF drawing speed 3 meters per minute): hexagonal geometry with shifted core [82, 83]; hexagonal geometry, that provides quasi-ring radial mode field distribution [82, 83]; equiangular spiral six-ray geometry [87, 88]. Further, by combining the maximal rotor rotation speed 200 revolutions per minute and low drawing speed 0.9 meter per minute, typical hexagonal geometry MOF with shifted core under pitch 0.65…0.700 and 3…4 spatial guided modes were

Preprints (www.preprints.org) | NOT PEER-REVIEWED | Posted: 25 May 2023 doi:10.20944/preprints202305.1814.v1

manufactured with twisting 217 rpm, which is finally the maximal possible induced chirality order for described above equipment.

Therefore, to improve MOF chirality, during the next stage, we have replaced installed stepper engine to new commutator motor with maximal rotation speed 2000 revolutions per minute, and carried out series of engineering and research and technological works on second set of drawing tower modifications [87, 88]. In addition to design, fabrication and installation of new carrier for motor fixing on the feed unit chuck, new drive belt with an improved length due to increasing the distance between the commutator motor shaft and feed unit chuck, new special supporting pad with the fixed commutator motor, protective shroud, and driving system in the drawing tower feed unit, outside control panel, connected to power supply and driver for commutator motor, we proposed and manufactured a special device for additional fixing of MOF cane to prevent its unacceptably strong vibrations in the horizontal plane with further destruction, occurring under a rotation speed of more than 300 revolutions per minute. This fixing device contains a ring stand with a clamped piece of fluoroplastic tube with a corresponding diameter, which was mounted between the tower feed unit and the tower furnace [87, 88].

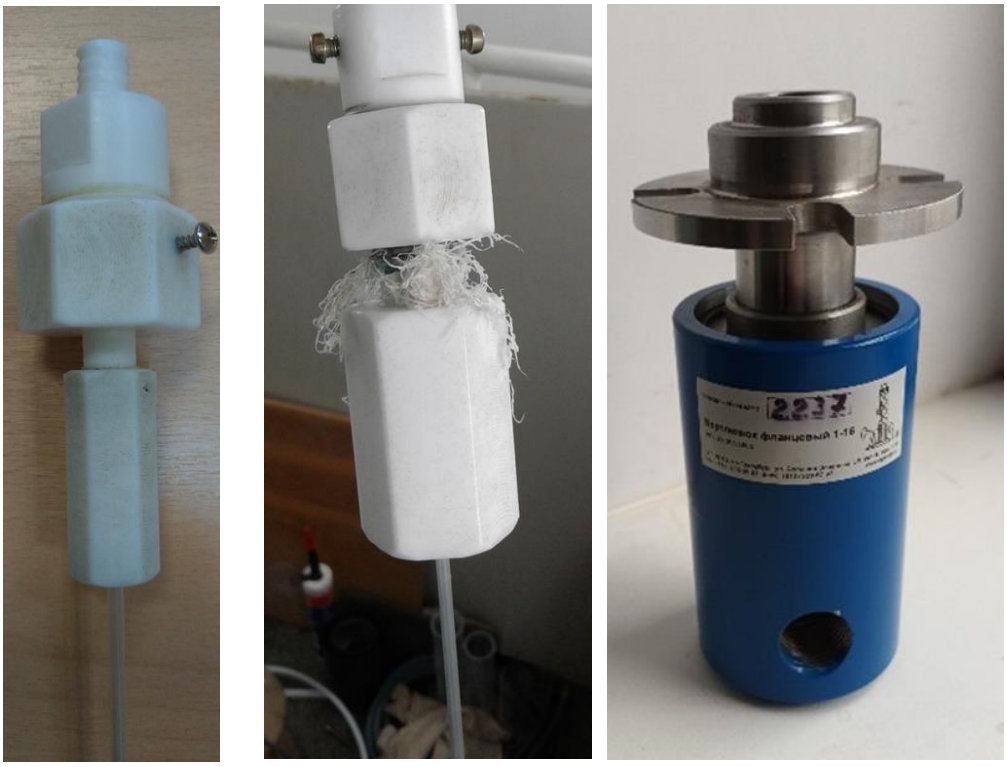

(a) (b) (c)

Figure 4. Adapters for excess pressure feeding to MOF cane capillaries under its rotation: (a) completed and jointed fluoroplastic rotational adapter with installed MOF cane; (b) destroyed fluoroplastic adapter under increased rotation speed of up to 600 revolutions per meter; (c) commercially available flanged drilling swivel, utilized instead previously installed fluoroplastic adapter.

As a result, the performed modifications provide improvements in the preform rotation speed in the drawing tower feed unit of up to 2000 revolutions per minute with twisting of up to 1000 rpm under a drawing speed of 2 meters per minute for silica few-mode optical fiber with typical “telecommunication” (“coaxial”) geometry (solid core, bounded by one outer solid cladding) and up to 500 rpm under the same drawing speed for MOFs.

By using developed technique, we have successfully fabricated pilot samples of silica few-mode MOFs with six GeO_2-doped cores and induced twisting of 50, 100, 400 and up to 500 rpm [87, 88]. However, further increase of rotation speed leads to progressive destruction (abrasion) of the mentioned above fluoroplastic rotational adapter over friction surfaces (Figure 4b), which disables it and blockages of MOF cane capillaries. Therefore,

Preprints (www.preprints.org) | NOT PEER-REVIEWED | Posted: 25 May 2023 doi:10.20944/preprints202305.1814.v1

during the next stage of drawing tower modification, we replaced fluoroplastic rotational adapter (Figure 4a,b) to commercially available flanged drilling swivel (Figure 4c), that provides feeding of excess pressure to cane capillaries under rotation speed 500…1000 revolutions per minute. This device enables gas feeding with pressure of up to 0.8 MPa with desired the maximal rotation speed of its spindle of 1000 revolutions per minute.

To provide precision movement of swivel relative to central axis of the drawing tower furnace flame space, we designed and fabricated special caprolon bracket, containing swivel movement system along Y-axis and device for its attachment, that provides swivel movement along X-axis with tight connection between cane and swivel. Also, special multicomponent sealed duralumin adapter tube was designed and manufactured to attach MOF cane to the feed unit chuck. The tube is fixed by chuck jaws, that provides rotation of drawn MOF. As a result, the swivel with adapter tube was mounted in the drawing tower feed unit by caprolon bracket (Figure 5a). Here the chuck of the feed unit is rotated by commutator motor via belt drive, while adapter tube is rotated via its fixation by chuck jaws (Figure 5b). The MOF cane is installed to the bottom of the adapter pipe, sub-pressed by hold-down nut and tighten by silicon sealing rubber. Described above configuration enables to feed excess pressure to MOF cane capillaries without its uncontrolled drop over attached unit, that provides desired chiral MOF drawing with cane rotation speed of up to 1000 revolutions per minute (Figure 5c).

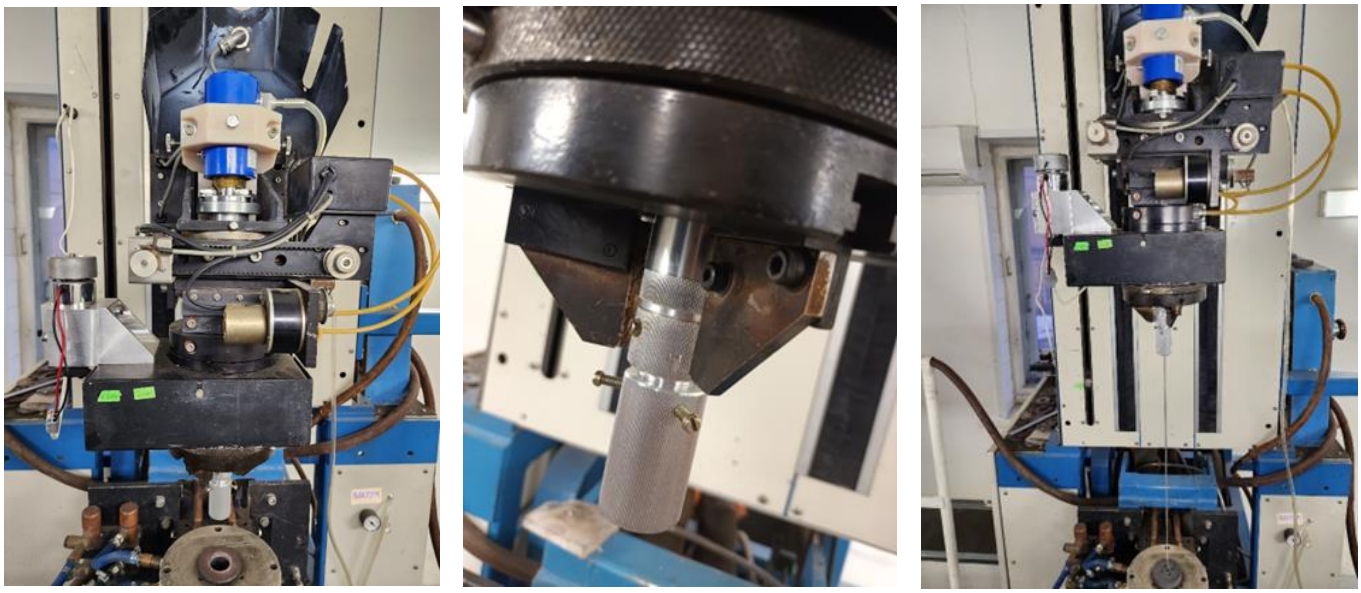

(a) (b) (c)

Figure 5. Modification of drawing tower feed unit: (a) caprolon bracket with swivel and adapter tube; (b) adapter tube fixation by chuck jaws in the feed unit; (c) the whole system, prepared for twisted MOF drawing with improved cane rotation speed of up to 1000 revolutions per minute.

5. Twisted Silica Few-Mode Hollow GeO_2-Doped Ring Core Microstructure Optical Fiber: Results

We successfully fabricated two samples of GeO_2-doped HRC MOF with and without induced chirality by typical three steps of MOF manufacturing technique [82, 83, 87, 88]: (1) MOF stack (preform) formation, (2) cane (pre-fiber) fabrication by re-drawing, and (3) drawing of MOF from the cane with optionally induced twisting.

During the first step, we re-drew high-purity fused synthetic silica supporting elements (rods and tubes with a content of hydroxyl groups (more 1000 ppm) to micro-rods and capillaries with an outer diameter of 1.37 mm and cut them into segments with lengths 30 cm long. Here we utilized cheap silica supporting tubes with a some OH^--group concentration (more than 1000 ppm—analog to the brands Heraeus Suprasil Standard, Saint-Gobain Spectrosil A and B, Corning HPFS 7980, JGS1, Dynasil 1100/Dynasil 4100,

Preprints (www.preprints.org) | NOT PEER-REVIEWED | Posted: 25 May 2023 doi:10.20944/preprints202305.1814.v1

Russian GOST 15130-86 "Optical quartz glass" KU-01, etc.), because the MCVD-process should be performed under low temperatures to prevent tube deformation and redundant evaporation of highly GeO_2-doped quartz near-surface layers, especially for large GeO_2-doped HRC preparation. Therefore, after a series of operations for the treatment of both capillaries and micro-rods (end melting in the flame of an oxyhydrogen torch under blowing by dried oxygen, chemical cleaning by concentrated hydrofluoric acid, washing by distilled water, drying in a muffle furnace, etc.), we formed an MOF stack by manually placing these prepared elements inside an 18 mm inner diameter silica substrate tube (Figure 6a), according to the desired cross-section geometry/structure (Figure 1) with central fabricated GeO_2-doped HRC-preform, and melted its end by using MCVD station.

During the second step, by using a drawing tower, we drew MOF cane (Figure 6b) with a length of 0.5 m and an outer diameter of 3 mm from the prepared stack under vacuum at 0.5 atm, with a feeding speed of 10 mm per minute, a drawing speed of 0.5 m per minute, and a drawing temperature of 1920°C [82, 83, 87, 88].

The third step contained the installation of prepared MOF cane into the feed unit of the drawing tower. Then it is driven into the high-temperature furnace and re-drawn to optical fiber under twisting provided by the installed commutator motor with swivel under drawing temperature of 1900°C, excess pressure 25 mbar and increased rotation speed of up to 1000 revolutions per minute. Therefore, we fabricated two samples of GeO_2-doped HRC MOF with outer diameter 65 μm, hollow ring core inner diameter 30.5 μm under wall thickness 1.7 μm and Δn=0.03: one untwisted (Figure 6c, e) and other with induced twisting of 790 rpm (Figure 6d, f) with length about 30 m.

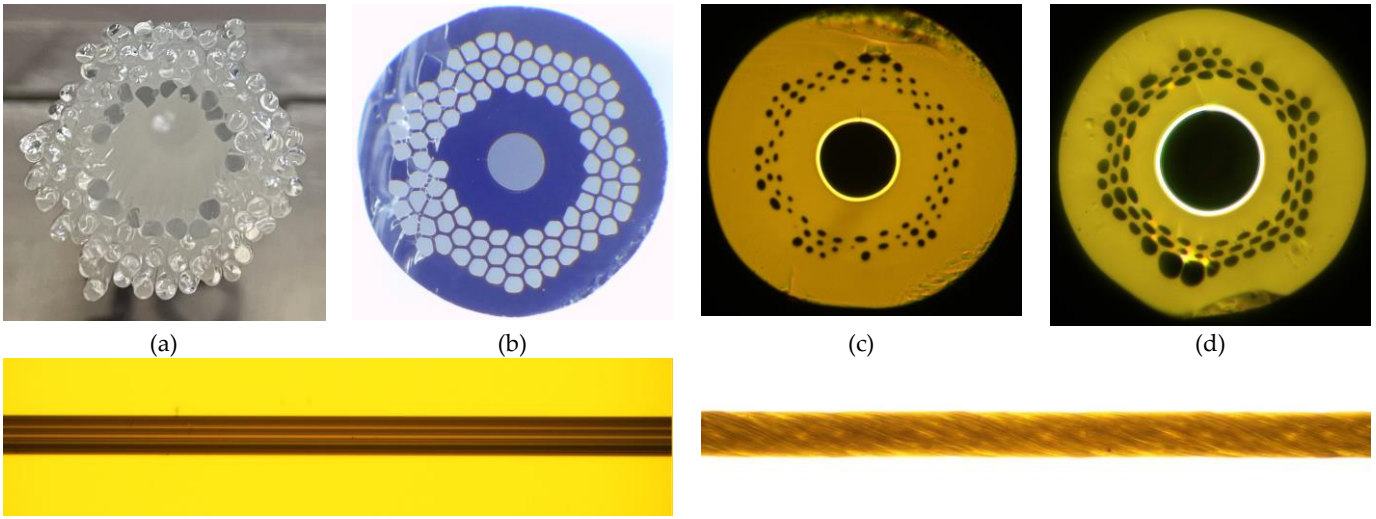

Figure 6. Silica GeO_2-doped HRC MOF: (a) stack; (b) cane; (c) cross-section of drawn untwisted GeO_2-doped HRC MOF; (d) cross-section of drawn GeO_2-doped HRC MOF with twisting 790 rpm; (e) longitudinal cross-section of untwisted HRC MOF; (f) longitudinal cross-section of spun HRC MOF with twisting 790 rpm.

Because the main attention was paid for HRC, the most part of holes in the MOF periphery part were deformed, while central part, containing HRC with surrounding area, kept its desired geometry.

Transmission spectra are presented on Fig. 7. We researched wavelength band λ=950…1700 nm by using a halogen lamp as a light source, programmable monochromator, germanium photodiode, optical amplifier, and optical power meter. Here lengths of both untwisted and twisted tested HRC MOF samples was 5 m. It is noticed, that for untwisted HRC MOF transmission wavelength range corresponds to short wavelengths and it is block already after λ=1300 nm, while twisted HRC MOF may transfer optical emission over all mentioned above tested wavelength band. We re-check this effect by the same

Preprints (www.preprints.org) | NOT PEER-REVIEWED | Posted: 25 May 2023 doi:10.20944/preprints202305.1814.v1

tests, performed for other 2 MOF samples, been cut from the opposite ends of drawn MOFs, but these measured spectra were analogously to Figure 7.

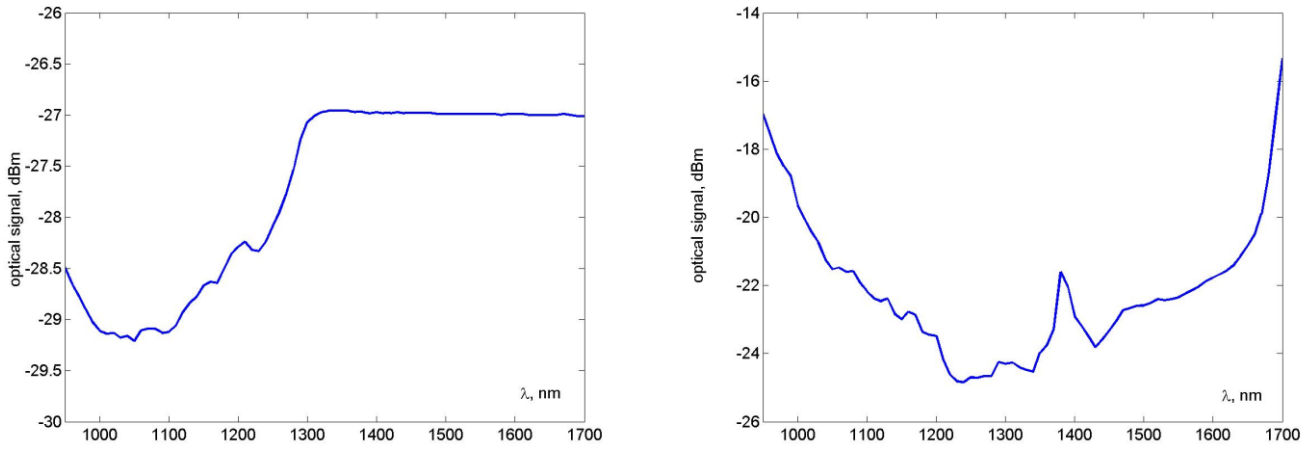

(a) (b)

Figure 7. Silica GeO_2-doped HRC MOF transmission spectra: (a) untwisted HRC MOF; (b) HRC MOF with twisting 790 rpm.

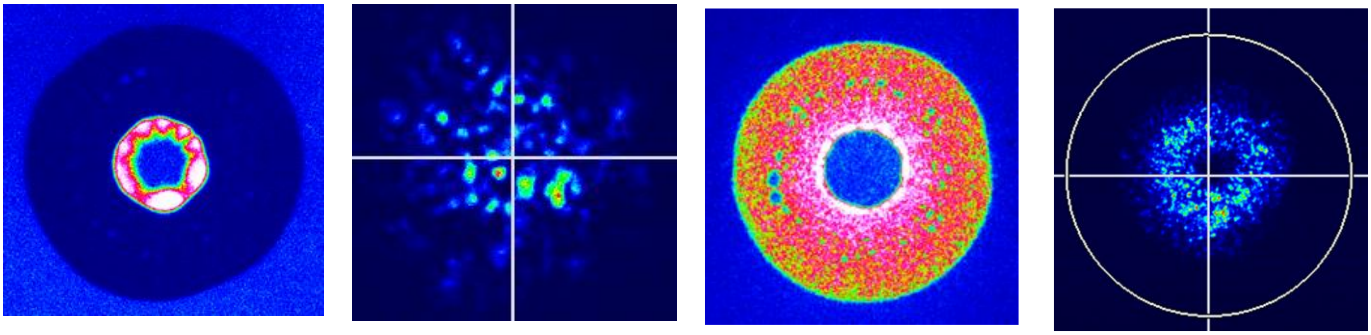

(a) (b) (c) (d)

Figure 8. Far-field laser beam profiles, measured at the receiving end after propagation over 5-meter long silica GeO_2-doped HRC MOF with ROFL launching conditions via MMF 50/125: (**a**) untwisted HRC MOF, "red" laser λ=650 nm; (**b**) untwisted HRC MOF, DFB laser λ=1550 nm; (**c**) 790 rpm, "red" laser λ=650 nm; (**d**) 790 rpm, DFB laser λ=1550 nm.

Results of the first test series, concerned with far-field laser beam profile measurements are shown on Fig. 8. Here we utilized "red" laser with operation wavelength λ=650 nm and DFB laser with operation wavelength λ=1550 nm. Here radially overfilled launching conditions via conventional multimode optical fiber (MMF) 50/125 pig-tail were provided, and it was connected to HRC MOF via free space by the field fusion splicer precision alignment system. According to measured images of laser beam profile at the receiving end after its propagation over 5-m long of tested HRC MOF, strongly twisted HRC MOF forms desired "donut" structure at both λ=650 nm and λ=1550 nm wavelengths, while untwisted HRC MOF provides ring radial mode field distribution at short wavelength λ=650 nm with falling apart to typical speckle pattern under long wavelength λ=1550 nm.

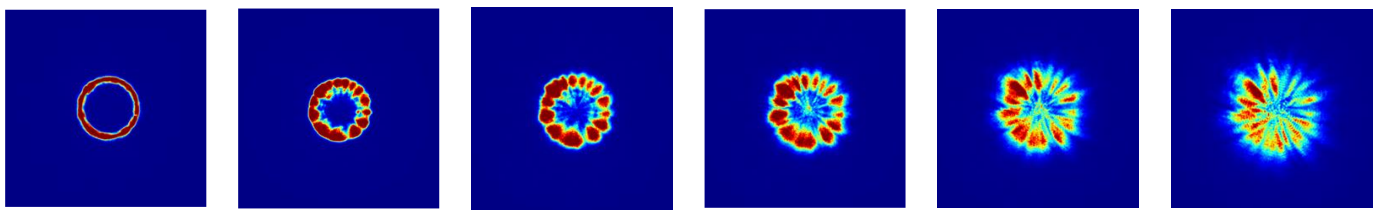

Preprints (www.preprints.org) | NOT PEER-REVIEWED | Posted: 25 May 2023 doi:10.20944/preprints202305.1814.v1

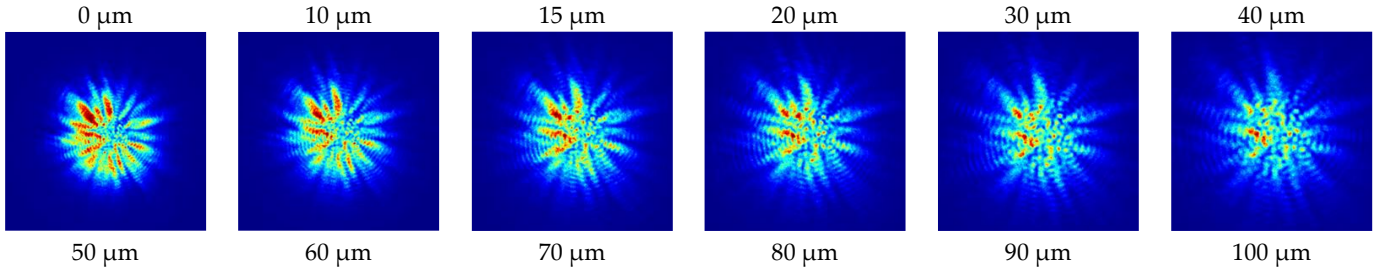

Figure 9. Dynamics of laser beam profile pattern, measured at the receiving end after propagation over 5-meter long untwisted HRC MOF, connected to "red" laser (λ = 1550 nm) via MMF centralized launching conditions over researched range of distance between MOF receiving end and IR-camera objective 0…100 μm.

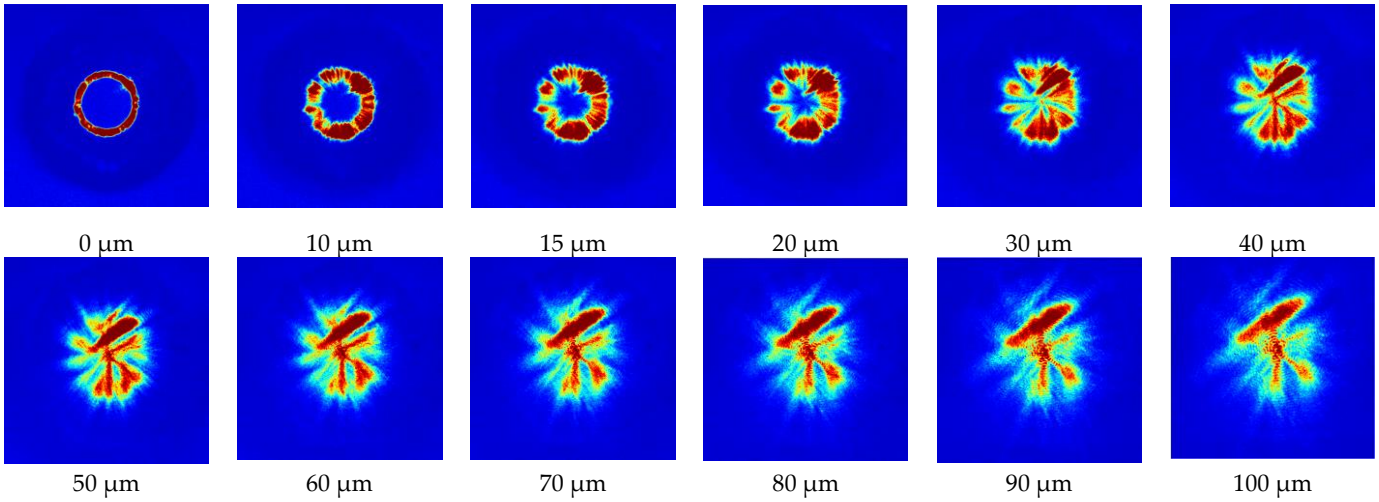

Figure 10. Dynamics of laser beam profile pattern, measured at the receiving end after propagation over 5-meter long 790-rpm-twisted HRC MOF, connected to "red" laser (λ = 1550 nm) via MMF centralized launching conditions over researched range of distance between MOF receiving end and IR-camera objective 0…100 μm.

The next test series was also focused on "red" laser (λ=650 nm) beam profile measurements after propagation over 5-m-long HRC MOF. However, here we provided centralized launching conditions also via MMF 50/125 pig-tail by fusion splicer alignment system under variation of distance between IR-camera objective and MOF receiving end-face. Therefore, 0 μm distance corresponded to maximal contrast of detected MOF end face image ("ring" due to centralized launching conditions – Fig. 9, Fig. 10 "0 μm"), while further distance increasing up to of 100 μm modified laser beam pattern and after 20 μm added some interferometric / optical vortex-like effects. It can be noticed, that under the mentioned distance between IR-objective – HRC MOF receiving end face 30 μm and more, untwisted HRC MOF laser beam profile contains speckle pattern, while 790-rpm- twisted HRC MOF represents stable "quasi-vortex" structure supposedly due to strongly improved mode coupling.

6. Conclusions

This work presents designed and first time successfully fabricated samples of silica few-mode twisted GeO_2-doped HRC MO with outer diameter 65 μm, HRC inner diameter 30.5 μm with GeO_2-doped wall thickness 1.7 μm and refractive index difference Δn=0.030, and strongly induced chirality with twisting up of to 790 rpm. Some technological issues are discussed, concerned with fabrication of GeO_2-doped supporting elements for large GeO_2-doped HRCs as well as of strongly twisted MOFs. We presented results of the tests, performed with pilot samples of described above designed and fabricated MOFs both

untwisted and twisted, including their geometrical parameters, basic transmission characteristics, as well as measurements of far-field laser beam profiles.

Experimentally verified, that strongly induced twisting of HRC MOF provides desired "donut" structure of radial mode field distribution superposition at both" short" ("red" λ=650 nm) and "long" (C-band center λ=1550 nm) wavelengths. It can be considered as some new type fiber optic diffractive element for mode filed management and summation / conversion. By analyzing a set of measured laser beam profiles, optimal launching conditions were detected: first of all, ROFL is required to provide desired mode field structure ("donut" vs "ring"). Increasing the distance between tested HRC MOF receiving end and camera objective up to of about 30 μm and more modifies and adds to beam profile pattern some interferometric effects.

Detailed research of the presented twisted few-mode GeO_2-doped HRC MOF properties for utilization in measurements/sensors or/and laser systems, telecommunications etc. require their customization for these applications as well as an additional series of tests and experiments in future works.

Author Contributions: Conceptualization, A.V.B., V.V.D., G.S., M.T., A.A.D., A.S.; methodology, A.V.B, V.V.D., E.V.T.-N., K.V.D..; investigation, A.V.B., V.V.D, A.V. Kh., A.S.M., A.I.K., G.A.P., E.V.T-N., D.N.S., S.V.B., M.V.D., A.S.E., E.S.Z., I.K.M., A.R.G., A.A.D., A.S.; validation, V.V.D, A.S.M., G.A.P., E.V.T-N., D.N.S., M.V.D., E.S.Z., A.A.V., A.R.G., I.K.M.; resources, A.V.B., K.V.D, M.V.D., A.A.V., V.S.E., M.T., G.S.; writing - original draft, A.V.B..; writing—review and editing, A.V.B.,V.V.D.; visualization, A.V.B., A.S., A.R.G., I.K.M., G.A.P., A.S.M.; supervision, A.V.B.; project administration, A.V.B. All authors have read and agreed to the published version of the manuscript.

Funding: This research received no external funding.

Institutional Review Board Statement: Not applicable.

Informed Consent Statement: Not applicable.

Data Availability Statement: The data presented in this study are available on request from the corresponding author. The data are not publicly available due to they are still collected, compared and analyzed for the set of fabricated pilot samples of twisted MOFs with various configuration.

Conflicts of Interest: The authors declare no conflict of interest. The funders had no role in the design of the study; in the collection, analyses, or interpretation of data; in the writing of the manuscript, or in the decision to publish the results.

References

1. Rusch, L.A.; Rad, M.; Allahverdyan, K.; Fazal, I.; Bernier, E. Carrying data on the orbital angular momentum of light. *IEEE Communication Magazines* **2018**, *56(2)*, 219 – 224.
2. Ma, M.; Lian, Yu.; Wang, Yu.; Lu, Zh. Generation, transmission and application of orbital momentum in optical fiber: a review. *Frontiers in Physics* **2021,** *9*, 77305-1 – 77305-15.
3. Wang, Zh.; Tu, Ji.; Gao, Sh.; Li, Zh.; Yu, Ch.; Lu, Ch. Transmission and generation of orbital angular momentum modes in optical fibers. *Photonics* **2021**, *8*, 246-1 – 246-24.
4. Choi, S.; Oh, K.; Shin, W.; Park, C.S.; Paek, U.C.; Park, K.J.; Chung, Y.C.; Kim, G.Y.; Lee, Y.G. Novel mode converter based on hollow optical fiber for Gigabit LAN communication. *IEEE Photonics Technology Letters* **2002**, *14(2)*, 248 – 250.
5. Oh, K.; Choi, S.; Shin, W. Applications of hollow core fibers. In Proceedings of the 16th Annual Meeting of the IEEE Lasers and Electro-Optics Society (LEOS), Tucson, Arizona, USA, 27-28 October 2003, 905 – 906.
6. Choi, S.; Shin, W.; Oh, K. Higher-order mode dispersion compensation technique based on mode converter using hollow optical fiber. In Proceedings of Optical Fiber Communication Conference (OFC), Anaheim, California, USA, 17 March 2002, 177 – 178.
7. Yue, Y.; Yan, Y.; Ahmed, N.; Yang, J.-Yu.; Zhang, L.; Ren, Yo.; Huang, H.; Birnbaum, K.; Erkmen, B.I.; Dolinar, S.; Tur, M.; Willner, A.E. Mode properties and propagation effects of optical orbital angular momentum (OAM) modes in a ring fiber. *IEEE Photonics Journal* **2012**, *4(2)*, 535 – 543.
8. Yan, Ho.; Zhang, E.; Duan, K. Free-space propagation of guided optical vortices excited in an annular core fiber. *Optics Express* **2012**, *20(16)*, 17904 – 17915.
9. Ramachandran, S.; Kristensen, P. Optical vortices in fiber. *Nanophotonics* **2013**, *2(5-6)*, 455 – 474.
10. Brunet, Ch.; Ung, B.; Wang, Li.; Messaddeq, Yo.; LaRochelle, S.; Rusch, L.A. Design of a family of ring-core fibers for OAM transmission studies. *Optics Express* **2015**, *23(8)*, 10553 – 10563.
11. Zhang, Xi; Chen, Shi; Wang, Ji. Weakly guiding graded-index ring-core fiber supporting 16-channel long distance mode division multiplexing systems based on OAM modes with low MIMO-DSP complexity. *Optics Express* **2022**, *30(20)*, 35828 – 35839.

12. Yang, J.; Wang, Y.; Fang, Y.; Geng, W.; Zhao, W.; Bao, C.; Ren, Y.; Wang, Z.; Liu, Y.; Pan, Z.; Yue, Y. Over-two-octave supercontinuum generation of light-carrying orbital angular momentum in Germania-doped ring-core fiber. *Sensors* **2022**, *22(6699)*, s22176699-1 – s22176699-11.
13. Geng, W.; Fang, Yu.; Wang, Yi.; Bao, Ch.; Wang, Zh.; Liu, Y.; Huang, H.; Ren, Yo.; Pan, Zh.; Yuie, Y. Highly dispersive Germanium-doped coupled ring-core fiber for vortex modes. *IEEE Journal of Lightwave Technology* **2022**, *40(7)*, 2144 – 2150.
14. Al-Zahrani, F.A.; Kabir, M.A. Ring-core photonic crystal fiber of terahertz orbital angular momentum modes with excellence guiding properties in optical fiber communication. *Photonics* **2021**, *8(122)*, 8040122-1 – 8040122-15.
15. Al-Zahrani, F.A.; Hassan, Md. M.; Enhancement of OAM and LP modes based on double guided ring fiber for high capacity optical communication. *Alexandria Engineering Journal* **2021**, *60*, 5065 – 5076.
16. Zhou, Ga.; Zhou, Gu.; Chen, Ch.; Xu, Mi.-N.; Xia, Ch.; Hou, Zh. Design and analysis of a microstructure ring fiber for orbital angular momentum transmission. *IEEE Photonics Journal* **2016**, 8*(2)*, 7802512-1 – 7802512-12.
17. Tian, W.; Zhang, H.; Zhang, X.; Xi, L.; Zhang, W.; Tang, X. A circular photonic crystal fiber supporting 26 OAM modes. *Optical Fiber Technology* **2016**, *30*, 184 – 189.
18. Zhang, H.; Zhang, Xi.; Li, H.; Deng, Y.; Xi, L.; Tang, Xi.; Zhang, W. The orbital angular momentum modes supporting fibers based on the photonic crystal fiber structure. *Crystals* **2017**, *7*, 7100286-1 – 7100286-15.
19. Bai, X.; Chen, H.; Yang, H. Design of a circular photonic crystal fiber with square air-holes for orbital angular momentum modes transmission. *Optics* **2018**, *158*, 1266 – 1274.
20. Xu, M.; Zhou, G.; Chen, Ch.; Zhou, G.; Sheng, Z.; Hou, Zh.; Xia, Ch. A novel micro-structured fiber for OAM mode and LP mode simultaneous transmission. *Journal of Optics* **2018**, *47(4)*, 428 – 436.
21. Debord, B.; Amrani, F.; Vincetti, L.; Gérôme, F.; Benabid, F. Hollow-core fiber technology: the rising of "gas photonics". *Fibers* **2018**, *7*, 7020016-1 – 7020016-58.
22. Hassan, Md. M.; Kabir, Md. A.; Hossain, Md. N.; Biswas, B.; Paul, B.; Ahmed, K. Photonic crystal fiber for robust orbital angular momentum transmission: design and investigation. *Optical and Quantum Electronics* **2020**, *52*, 8-1 – 8-14.
23. Huang, W.; You, Yo.; Song, B.-B.; Chen, Sh.-Yo. A photonic crystal fiber for supporting 30 orbital angular momentum modes with low dispersion. *Optoelectronics Letters* **2020**, *16(1)*, 0034 – 0039.
24. Ke, X.; Wang, S. Design of photonic crystal fiber capable of carrying multiple orbital angular momentum modes transmission. *Optics and Photonics Journal* **2020**, *10*, 49 – 63.
25. Hong, S.; Lee, Y.S.; Choi, H.; Quan, C.; Li, Y.; Kim, S.; Oh, K. Hollow silica photonic crystal fiber guiding 101 orbital angular momentum modes without phase distortion in C + L band. *IEEE Journal of Lightwave Technology* **2020**, *38(5)*, 1010 – 1018.
26. Zhao, L.; Zhao, H.; Xu, Z.; Liang, R. A Design of novel photonic crystal fiber with low and flattened dispersion for supporting 84 orbital angular momentum modes. *Communications in Theoretical Physics* **2021**, *73*, 085501-1 – 085501-15.
27. Rjeb, A.; Fathallah, H.; Chebaane, S.; Machhout, M. Design of novel circular lattice photonic crystal fiber suitable for transporting 48 OAM modes. *Optoelectronics Letters* **2021**, *17(8)*, 0501 – 0506.
28. Liu, Ch.; Fu, H.; Hu, Ch.; Zhou, L.; Shi, Yi.; Lv, J.; Yang, L.; Chu, P.K. Optimization of photonic crystal fibers for transmission of orbital angular momentum modes. *Optical and Quantum Electronics* **2021**, *53*, 639-1 – 639-18.
29. Li, J.; Li, H.; Wang, Z. Application of hollow-core photonic crystal fibers in gas Raman lasers operating at 1.7 μm. *Crystal* **2021**, *11*, 11020121-1 – 11020121-15.
30. Fu, H.; Shi, Y.; Yi, Z.; Liu, Ch.; Song, X.; Lv, J.; Yang, L. Effects of air holes in the cladding of photonic crystal fibers on dispersion and confinement loss of orbital angular momentum modes. *Optical and Quantum Electronics* **2022**, *54*, 353-1 – 353-17.
31. Sun, Yu.; Lu, W.; Liu, Q.; Lv, J.; Tai, Sh.; Han, M., Chu, P.K., Liu, Ch. A large effective mode area photonic crystal fiber supporting 134 OAM modes. *Journal of Optics* **2023**, *2023*, s12596-1 – s12596-10.
32. Belardi, W. Design and properties of hollow antiresonant fibers for the visible and near infrared spectral range. *IEEE Journal of Lightwave Technology* **2015**, *33(21)*, 4497 – 4503.
33. Bufetov, I.A.; Kosolapov, A.F.; Pryamikov, A.D.; Gladyshev, A.V.; Kolyadin, A.N.; Krylov, A.A.; Yatsenko, Yu.P.; Biriukov, A.S. Revolver hollow core optical fibers. *Fibers* **2018**, *6*, 6020039-1 - 6020039-26.
34. Chafer, M.; Osório, J.H.; Amrani, F.; Delahaye, F.; Maurel, M.; Debord, B.; Gérôme, F.; Benabid, F. 1 km hollow-core fiber with loss at the silica Rayleigh limit in the green spectral region. *IEEE Photonics Technology Letters* **2019**, *31(9)*, 685 – 688.
35. Sakr, H.; Chen, Yo.; Jasion, G.T., Bradley, Th.D.; Hayes, J.R.; Mulvad, H.Ch.H.; Davidson, I.A.; Fokoua, N.; Poletti, F. Hollow core optical fibres with comparable attenuation to silica fibres between 600 and 1100 nm. *Nature* **2020**, *11*, 6030-1 – 6030-10.
36. Pierscinski, K.; Stepniewski, Gr.; Klimczak, M.; Sobczak, Gr.; Dobrakowski, D.; Pierscinska, D.; Pysz, D.; Bugajski, M.; Buczynski, R. Butt-coupling of 4.5 μm quantum cascade lasers to silica hollow core anti-resonant fibers. *IEEE Journal of Lightwave Technology* **2021**, *39(10)*, 3284 – 3290.
37. Tsiminis, G.; Rowland, K.J.; Schartner, E.P.; Spooner, N.A.; Monro, T.M.; Ebendorff-Heidepriem, H. Single-ring hollow core optical fibers made by glass billet extrusion for Raman sensing. *Optics Express* **2016**, *24(6)*, 5911 – 5917.
38. Tu, Ji.; Gao, Sh.; Wang, Zh.; Liu, Zh.; Li, W.; Du, Ch.; Liu, W.; Li, Zh.; Yu, Ch.; Tam, H.; Lu, Ch. Bend-insensitive grapefruit-type holey ring-core fiber for weakly-coupled OAM mode division multiplexing transmission. *IEEE Journal of Lightwave Technology* **2020**, *38(16)*, 4497 – 4503.
39. Cubillas, A.M.; Jiang, X.; Euser, T.G.; Taccardi, N.; Etzold, B.J.M.; Wasserscheid, P.; Russell, Ph. St. J. Photochemistry in a soft-glass single-ring hollow-core photonic crystal fibre. *The Royal Society of Chemistry. Analyst* **2017**, *142*, 925 – 929.

40. Huang, Sh.-H.; Ma, Qi-Ch.; Chen, W-Ch.; Liu, H.-Zh.; Xing, Xi.-Bo; Cui, Hu; Luo, Zh.-Ch.; Xu, W.-Ch.; Luo, Ai-P. Microstructure ring fiber for supporting higher-order orbital angular momentum modes with flattened dispersion in broad waveband. *Applied Physics B. Lasers and Optics* **2019,** *125*, 197-1 – 197-8.
41. Ma, Q.; Luo, A.P.; Hong, W. Numerical study of photonic crystal fiber supporting 180 orbital angular momentum modes with high mode quality and flat dispersion. *IEEE Journal of Lightwave Technology* **2021**, *39(9)*, 2971 – 2979.
42. Fu, H.; Liu, Ch.; Yi, Z; Song, Xi.; Li, Xi.; Zeng, Ya.; Wang, Ji.; Lv, Ji.; Yang, L.; Chu, P.-K. A new technique to optimize the properties of photonic crystal fibers supporting transmission of multiple orbital angular momentum. *Journal of Optics* **2023**, *52(1)*, 307 – 316.
43. Wang, Yi.; Zhao, We.; Geng, We.; Fang, Yu.; Bao, Ch.; Wang, Zh.; Zhang, H.; Ren, Yo.; Wang, Zh.-Yi.; Pan, Zh.; Yue, Ya. Air-core ring fiber guiding >400 radially fundamental OAM modes across S+C+L bands. *IEEE Access* **2021,** *9*, 75617 – 75625.
44. Wang, Yi.; Lu, Ya.; Bao, Ch.; Geng, We.; Fang, Yu.; Mao, Ba.; Wang, Zh.; Liu, Ya.; Huang, H.; Ren, Yo.; Pan, Zh. Hollow ring-core photonic crystal fiber with >500 OAM modes over 360-nm communication bandwidth. *IEEE Access* **2021,** *9*, 66999 – 67005.
45. Wang, Yi.; Bao, Ch.; Geng, We.; Lu, Y.; Fang, Yu.; Mao, Ba.; Liu, Y., Liu, B., Huang, H.; Ren, Yo.; Pan, Zh.; Yue, Ya. Air-core ring fiber with >1000 radially fundamental OAM modes across O+E+S+C+L bands. *IEEE Access* **2020,** *8*, 68280 – 68287.
46. Gregg, P.; Kristensen, P.; Golowich, E.; Olsen, J.O.; Steinvurzel, P.; Ramachandran, S. Stable transmission of 12 OAM states in air-core fiber. In Proceedings of the Conference on Lasers and Electro-Optics (CLEO), San Jose, California, USA, 9 – 14 June 2013, CTu2K.2-1 - CTu2K.2-2.
47. Gregg, P.; Kristensen, P.; Ramachandran, S. Conservation of orbital angular momentum in air-core optical fibers. *Optica* **2015**, *2(3)*, 267 – 270.
48. Kang, Qi.; Gregg, P.; Jung, Yo.; Lim, E.L.; Alam, Sh.; Ramachandran, S.; Richardson, D.J. Amplification of 12 OAM States in an Air-Core EDF. In Proceedings of Optical Fiber Communication Conference (OFC), Los Angeles, California, USA, 22 – 26 March 2015, Tu3C.2-1 - Tu3C.2-3.
49. Gregg, P.; Kristensen, P.; Ramachandran, S. 13.4km OAM state propagation by recirculating fiber loop. *Optics Express* **2016**, *24(17)*, 18938 – 18947.
50. Gregg, P.; Kristensen, P.; Rubano, A.; Golowich, S.; Marrucci, L.; Ramachandran, S. Enhanced spin orbit interaction of light in highly confining optical fibers for mode division multiplexing. *Nature Communications* **2019**, *10*, 4707-1 – 4707-8.
51. Bozinovic, N.; Yue, Y.; Ren, Y.; Tur, M.; Kristensen, P.; Huang, H.; Willner, A.E.; Ramachandran, S. Terabit-scale orbital angular momentum mode division multiplexing in fibers. *Science* **2013**, *340*, 1545 – 1548.
52. Brunet, Ch.; Vaity, P.; Messaddeq, Yo.; LaRochelle, S.; Rush, L.A. Design, fabrication and validation of an OAM fiber supporting 36 states. *Optics Express* **2014**, *22(21)*, 26117 – 26127.
53. Rush, L.A.; Larochelle, S. Fiber transmission demonstrations in vector mode space division multiplexing. *Frontiers of Optoelectronics* **2018**, *11(2)*, 155–162.
54. Tu, J.; Liu, Zh.; Gao, Sh.; Wang, Zh.; Zhang, J.; Zhang, B.; Li, J.; Liu, W.; Tam, H.; Li, Zh.; Yu, Ch.; Lu, Ch. Ring-core fiber with negative curvature structure supporting orbital angular momentum modes. *Optics Express* **2019**, *27*, 20358–20372.
55. Tu, J.; Gao, S.; Wang, Z.; Liu, Z.; Li, W.; Du, C.; Liu, W.; Li, Z.; Yu, C.; Tam, H.; et al. Bend-insensitive grapefruit-type holey ring-core fiber for weakly-coupled OAM mode division multiplexing transmission. IEEE Journal of Light Technology **2020**, *38*, 4497–4503.
56. Xi, X.M.; Wong, G.K.L.; Weiss, T.; Russell, P.S.J. Measuring mechanical strain and twist using helical photonic crystal fiber. *Optics Letters*. **2013**, *38*, 5401–5404.
57. Napiorkowski, M.; Zolnacz, K.; Statkiewicz-Barabach, G.; Bernas, M.; Kiczor, A.; Mergo, P.; Urbanczyk, W. Twist induced mode confinement in partially open ring of holes. *IEEE Journal of Lightwave Technology* **2020**, *38*, 1372–1381.
58. Zhang, M.; Zhang, L.; Chen, O.; Bai, G.; Li, S. A designed twist sensor based on the SPR effect in the thin-gold-film-coated helical microstructured optical fibers. *Sensors* **2022**, *22*, 5668.
59. Bohnert, K.; Gabus, P.; Kostovic, J.; Brandle, H. Optical fiber sensors for the electric power industry. *Opt. Lasers Eng.* **2005**, *43*, 511–526.
60. Weiss, T.; Wong, G.K.L.; Biancalana, F.; Barnett, S.M.; Xi, X.M.; Russell, P.S.J. Topological Zeeman effect and circular birefringence in twisted photonic crystal fibers. *Journal of Optical Society of America B* **2013**, *30*, 2921–2927.
61. Xi, X.M.; Weiss, T.; Wong, G.K.L.; Biancalana, F.; Barnett, S.M.; Padgett, M.J.; Russell, P.S.J. Optical activity in twisted solid-core photonic crystal fibers. *Physics Review Letters* **2013**, *110*, 143903.
62. Wong, G.K.L.; Xi, X.M.; Frosz, M.H.; Russell, P.S. J. Enhanced optical activity and circular dichroism in twisted photonic crystal fiber. *Optical Letters* **2015**, *40*, 4639–4642.
63. Alexeyev, C.N.; Lapin, B.P.; Milione, G.; Yavorsky, M.A. Optical activity in multihelicoidal optical fibers. *Physical Review A* **2015**, *92*, 033809.
64. Alexeyev, C.N.; Lapin, B.P.; Milione, G.; Yavorsky, M.A. Resonance optical activity in multihelicoidal optical fibers. *Optics Letters* **2016**, *41*, 962–965.
65. Napiórkowski, M.; Urbanczyk, W. The effect of coupling between core and cladding modes in twisted microstructured optical fibers. *Proceedings of SPIE* **2018**, *10681*, 106810H-1 – 106810H-8.
66. Ma, X.; Zhu, C.; Hu, I.-N.; Kaplan, A.; Galvanauskas, A. Single-mode chirally-coupled-core fibers with larger than 50 μm diameter cores. *Optics Express* **2014**, *22*, 9206–9219
67. Wong, G.K.L.; Kang, M.S.; Lee, H.W.; Biancalana, F.; Conti, C.; Weiss, T.; Russell, P.S.J. Excitation of orbital angular momentum resonances in helically twisted photonic crystal fiber. *Science* **2012**, *vol. 337*, 446 – 449.

68. Barshak, E.V.; Alexeyev, C.N.; Lapin B.P.; Yavorsky, M.A. Twisted anisotropic fibers for robust orbital-angular-momentum-based information transmission. *Physical Review A*. **2015**, *vol. 91*, 033833-1 – 033833-10.
69. Chattopadhyay, R.; Biswas, T.; Bhadra, Sh.K. Light propagation at Dirac point in twisted photonic crystal. In Proceedings of 13th International Conference on Fiber Optics and Photonics, Kanpur, India, 4 – 8 December 2016.
70. Cui, Y.; Ye, J.; Li, Y.; Dai, P.; Qu, Sh. Vortex chirality-dependent filtering in helically twisted single-ring photonic crystal fibers. *Optics Express* **2019**, *27(15)*, 20816 – 20823.
71. Vigneswaran, Dh.; Rajan, M.S.M.; Biswas, B.; Grover, A.; Ahmed, K.; Paul, B.K. Numerical investigation of spiral photonic crystal fiber (S-PCF) with supporting high order OAM modes propagation for space division multiplexing applications. *Optical and Quantum Electronics* **2021**, *53*, 78-1 – 78-11.
72. Russel, P.St.J.; Beravat, R.; Wong, G.K.L. Helically twisted photonic crystal fibres. *Philosophical Transactions A. Royal Society* **2017**, *375*, 20150440-1 – 20150440-18.
73. Xi, X.M.; Wong, C.K.L.; Frosz, M.H.; Babic, F.; Ahmed, G.; Jiang, X.; Euser, T.G.; Russel, P.St.J. Orbital-angular-momentum-preserving helical Bloch modes in twisted photonic crystal fiber. *Optica* **2014**, *1(3)*, 165 – 169.
74. Stefani, A.; Kuhlmey, B.T.; Fleming, S. Orbital angular momentum modes by twisting of a hollow core antiresonant fiber. In Proceedings of European Conference on Lasers and Electro-Optics and European Quantum Electronics Conference (CLEO/Europe-EQEC), Munich, Germany, 25 – 29 June 2017.
75. Stefani, A.; Fleming, S.C.; Kuhlmey, B.T. Terahertz orbital angular momentum modes with flexible twisted hollow core antiresonant fiber. *APL Photonics* **2018**, *vol. 3*, 051708-1 – 051708-11.
76. Fu, C.; Liu, Sh.; Wang, Y.; Bai, Zh., He, J.; Liao, Ch.; Zhang, C.; Zhang, F.; Yu, B.; Gao, Sh.; Li, Zh.; Wang, Y. High-order orbital angular momentum mode generator based on twisted photonic crystal fiber. *Optics Letters* **2018**, *vol. 43(8)*, 1786 – 1789.
77. Zhou, G.; Liu, J.; Changming Xia, Ch.; Hou, Zh. Orbital-angular-momentum-amplifying helical vector modes in Yb3+-doped three-core twisted microstructure fiber. *Optics Express* **2020**, *28(14)*, 21110 – 221119.
78. Adams, M.J. *An Introduction to Optical Waveguides*, John Wiley & Sons Ltd.: New York, USA, 1981, ISBN-13: 978-0-4712-7969-3.
79. Binh, L.N., Design guidelines for ultra-broadmand dispersion-flattened optical fibers with segmented-core index profile, Technical Report MECSE-14-2003, Clayton, Australia, 2003.
80. Fleming, J.W. Dispersion in GeO_2-SiO_2 glasses, *Applied Optics* **1984**, *23(24)*, 4886 – 4493.
81. Burdin, V.A. Methods for computation of Sellmeier coefficients for dispersion analysis of silica optical fibers, *Infocommunikacionnye Technologii (Infocommunication Technologies)* **2006**, *4(2)*, 30 – 34.
82. Bourdine, A.V.; Burdin, V.A.; Demidov, V.V.; Dukelskii, K.V.; Gizatulin, A.R.; Khokhlov, A.V.; Meshkov, I.K.; Sultanov, A.Kh.; Ter-Nersesyants, E.V.; Ustinov S.V.; Zaitseva, E.S. Design of vortex optical fibers for RoF systems: Part II: pilot samples of chiral microstructured optical fibers *Proceedings of SPIE* **2020**, *11516*, 115161T-1 – 115161T-7.
83. Bourdine, A.V.; Barashkin, A.Yu.; Burdin, V.A.; Dashkov, M.V.; Demidov, V.V.; Dukelskii, K.V.; Evtushenko, A.S.; Ismail, Y.; Khokhlov, A.V.; Kuznetsov, A.A.; Matrosova, A.S.; Morozov, O.G.; Pchelkin, G.A.; Petruccione, F.; Sakhabutdinov, A.Zh.; Singh, G.; Ter-Nersesyants, E.V; Tiwari, M.; Zaitseva, E.S.; Janyani, V.; Yin, J. Twisted silica microstructured optical fiber with equiangular spiral six-ray geometry, *Fibers* **2021**, *9(27)*, fib9050027-1 - fib9050027-17.
84. Bourdine, A.V.; Demidov, V.V.; Kuznetsov, A.A.; Vasilets, A.A.; Ter-Nersesyants, E.V.; Khokhlov, A.V.; Matrosova, A.S.; Pchelkin, G.A.; Dashkov, M.V.; Zaitseva, E.S.; Gizatulin, A.R.; Meshkov, I.K.; Sakhabutdinov, A.Zh.; Dmitriev, E.V.; Morozov, O.G.; Burdin, V.A.; Dukelskii, K.V.; Ismail, Y.; Petruccione, F.; Singh, G.; Tiwari, M.; Yin, J. Twisted few-mode optical fiber with improved height of quasi-step refractive index profile. *Sensors* **2021**, *22(9)*, 3124-1 – 3124-15.
85. Bourdine, A.V.; Dashkov, M.V.; Kuznetsov, A.A.; Demidov, V.V.; Evtushenko, A.S.; Barashkin, A.Yu.; Ter-Nersesyants, E.V.; Vasilets, A.A.; Morozov, O.G.; Burdin, V.A.; Dukelskii, K.V.; Sakhabutdinov, A.Zh.; Zaitseva, E.S.; Gizatulin, A.R.; Meshkov, I.K.; Dmitriev, E.V.; Ismail, Y.; Petruccione, F.; Singh, G.; Tiwari, M.; Yin, J. Pulse and spectral responses of laser-excited twisted silica few-mode optical fiber with improved height of quasi-step refractive index profile. *Proceedings of SPIE* **2021**. *12295*, 1229509-1– 1229509-11.
86. Bourdine, A.V.; Barashkin, A.Yu.; Burdin, V.A.; Dashkov, M.V.; Demidov, V.V.; Khokhlov, A.V.; Ter-Nersesyants, E.V.; Matrosova, A.S.; Pchelkin, G.A.; Dukelskii, K.V.; Evtushenko, A.S.; Zaitseva, E.S.; Ismail, Y.; Kuznetsov, A.A.; Morozov, O.G.; Sakhabutdinov, A.Zh.; Petruccione, F.; Singh, G.; Tiwari, M.; Janyani, V. Researches of parameters of chiral few-mode optical fiber pilot sample with improved height of step refractive index profile. *Proceedings of Telecommunication Universities* **2021**, *7(1)*, 37 – 49.
87. Pchelkin, G.A.; Demidov, V.A.; Ter-Nersesyants, E.V.; Khokhlov, A.V.; Bourdine, A.V.; Matrosova, A.S.; Dukelskii, K.V.; Davydov, V.V.; Podoprigora, A.N.; Pilipova, V.M.; Shurupov, D.A.; Romashova, V.B.; Kashina, R.R. Study of the characteristics of few-mode microstructured optical fibers with 6 cores, made of highly doped GeO2 silica and induced chirality. In Proceedings of IEEE 2022 International Conference on Electrical Engineering and Photonics (EExPolytech-2022), St. Petersburg, Russia, 20 – 21 October 2022
88. Bourdine, A.V.; Demidov, V.A.; Dukelskii, K.V.; Khokhlov, A.V.; Ter-Nersesyants, E.V.; Bureev, S.V.; Matrosova, A.S.; Pchelkin, G.A.; Kuznetsov, A.A.; Morozov, O.G.; Nureev, I.Il.; Sakhabutdinov, A.Zh.; Agliullin, T.A.; Dashkov, M.V.; Evtushenko, A.S.; Zaitseva, E.S.; Vasilets, A.A.; Gizatulin, A.R.; Meshkov, I.K.; Ismail, Y.; Petruccione, F.; Singh, G.; Tiwari, M.; Yin J. Six-core GeO2-doped silica microstructured optical fiber with induced chirality. Fibers **2023**, *11(3)*, 28-1 – 28-1.